Chemistry Europe
European Chemical Societies Publishing

WILEY VCH

Excellence in Chemistry Research

Announcing our new flagship journal

- Gold Open Access
- Publishing charges waived
- Preprints welcome
- Edited by active scientists

Meet the Editors of *ChemistryEurope*

Luisa De Cola
Università degli Studi di Milano Statale, Italy

Ive Hermans
University of Wisconsin-Madison, USA

Ken Tanaka
Tokyo Institute of Technology, Japan

ChemPlusChem

A Multidisciplinary Journal Centering on Chemistry

Chemistry Europe

European Chemical Societies Publishing

Accepted Article

Title: The Role of a Sn Promoter on an Anodic Pt Electrocatalyst Prepared over H2O2-Functionalized Carbon Supports for Direct Ethanol Fuel Cell (DEFC) Applications

Authors: M. Florencia Azcoaga Chort, Julieta Stassi, Sergio de Miguel, Natalia Veizaga, and Virginia Rodriguez

To be cited as: *ChemPlusChem* **2023**, e202300089

Link to VoR: https://doi.org/10.1002/cplu.202300089

WILEY VCH

RESEARCH ARTICLE WILEY-VCH

The Role of a Sn Promoter on an Anodic Pt Electrocatalyst Prepared over H_2O_2-Functionalized Carbon Supports for Direct Ethanol Fuel Cell (DEFC) Applications

María Florencia Azcoaga Chort, Julieta Paola Stassi, Sergio Rubén de Miguel, Natalia Soledad Veizaga*, and Virginia Inés Rodríguez*

[a] M.F. Azcoaga Chort, Dr. J.P. Stassi, Dr. S.R. de Miguel, Dr. N.S. Veizaga, Dr. V.I. Rodríguez
Instituto de Investigaciones en Catálisis y Petroquímica "Ing. José Miguel Parera" (INCAPE)
UNL-CONICET
3000 - Santa Fe, Argentina
E-mail: nveizaga@fiq.unl.edu.ar
virodri@fiq.unl.edu.ar

Supporting information for this article is given via a link at the end of the document.

Abstract: Multiwalled carbon nanotubes and Vulcan carbon were functionalized with a 30 %v/v hydrogen peroxide solution and employed as supports for Pt and PtSn catalysts prepared by the polyol method. PtSn catalysts with a Pt loading of 20 wt.% and a Pt:Sn atomic ratio equal to 3:1 were evaluated in the ethanol electrooxidation reaction. The effects of the oxidizing treatment on the surface area and the surface chemical nature were analyzed through N_2 adsorption, isoelectric point, and temperature-programmed desorption measurements. Results showed that the H_2O_2 treatment affects the surface area of the carbons to a great extent. Characterization results indicated that the performance of the electrocatalysts strongly depends both on the presence of Sn and on the support functionalization. PtSn/CNT-H_2O_2 electrocatalyst displays a high electrochemical surface area and enhanced catalytic activity for ethanol oxidation in comparison to other catalysts in the present study.

Introduction

The fuel cell is an innovative device that converts chemical energy into electrical energy with high efficiency, adaptability, and ease of construction. As a result, fuel cells have gained significant attention for their potential to promote efficient resource utilization and pollution control. They work by utilizing catalysts to transform fuel molecules and oxidants into ions that migrate through the electrolyte, generating voltage for power supply. Developing high-performance anodic fuel oxidation and cathodic oxygen reduction catalysts can enhance the catalytic performance and accelerate their industrialization. Fuel cells have been investigated with various types of fuels, including liquid fuels that have advantages such as abundant raw materials, convenient transportation, and low cost, making them a promising energy carrier for the anodic process. Compared to hydrogen fuel, liquid fuels can overcome the limitations of limited sources and difficult storage.[1-8]

The ethanol oxidation reaction (EOR) process involves 12 e- transfer and C-C bond cleavage. It features several reaction steps with the formation of intermediates and by-products. They have been widely studied and recognized as the "dual pathway" mechanism by the C1 and C2 pathways, respectively. The C1 pathway mainly involves the cleavage of C-C and the formation of CO_{ads}. The CO_{ads} would react with OH_{ads} to produce CO_2. Conversely, the C2 pathway refers to the formation of various intermediates from $(CH_3CH_2O\text{-})_{ads}$, $(CH_3CO)_{ads}$, and other species without breaking the C-C bond, yielding acetic acid or acetate.[7] Pure Pt catalysts are not efficient for EOR due to the fact that Pt is quickly poisoned by the CO intermediate species. For this reason, the formulation of bi and trimetallic catalysts based on Pt has been extensively studied.[9-32] Selecting Sn as the second metal, PtSn over various carbon nanocomposites has been investigated. These catalysts have been prepared through the use of diverse deposition methods and used as anodic electrocatalysts for the oxidation of low molecular weight alcohols and other small fuel molecules[13-16,25,33-44] obtaining different results.

Furthermore, to improve the electrocatalytic performance, it is desirable to enhance the metallic dispersion in carbon-supported catalysts. To achieve this goal, it is possible to employ supports with a high surface area showing a high number of anchoring sites. Also, oxidative treatments (nitric and citric acids, ammonium persulfate, and hydrogen peroxide -H_2O_2-) could improve the performance of electrocatalysts [45-53] and catalysts for hydrogenation and oxidation reactions.[54-58] It has been observed that the presence of oxygenated surface groups influences carbon surface behavior.[40,54,58] For the correct fixation of –OH groups, hydrogen peroxide is the most frequently used acidic agent. Both Marega et al.[59] and Avilés et al.[60] studied the effect of strong and weak acids on the functionalization and structural damage of the carbon nanotubes. They reported that the use of weak acids such as H_2O_2 provides, in comparison to HCl, HNO_3, and H_2SO_4, better control over the shortening and uncapping of the nanotubes avoiding dramatical deterioration of the structural integrity. Safo et al.[61] found out that not only does H_2O_2 oxidation generate surface oxygen-containing groups but it also creates defects on the surface. The size of carbon nanotubes gradually decreased with the increase of oxidation time as evidenced by scanning electron microscopy images. Temperature-programmed desorption measurements showed that the oxidation with H_2O_2 promotes the formation of CO-related oxygen groups (phenol, carbonyl quinones and ether) rather than the formation of CO_2-related oxygen groups (lactone and carboxyl). The carboxylic anhydrides formation was only detected when the treatment was carried out at 25 ºC for a period longer than 4 weeks. Carmo et al.[45] observed a higher

activity of the PtRu/H_2O_2-C catalyst compared to PtRu/untreated-C in cyclic voltammetry curves. They attributed this result to a better distribution of the metal on the H_2O_2-functionalized carbon.

The objective of this work is to functionalize multiwalled carbon nanotubes (CNT) and Vulcan carbon (VC) proficiently without causing them considerable structural damage in order to employ them as supports for Pt and PtSn catalysts in the ethanol oxidation reaction.

Results and Discussion

Figure 1a presents the temperature-programmed desorption (TPD) profiles of the functionalized and non-functionalized supports. In the case of both non-functionalized supports, a very low (or even non existing) desorption of acid surface groups is observed. Functionalization with hydrogen peroxide generates a moderate amount of strong acid surface groups that desorb CO_2 at temperatures between 200 and 400 °C, and it also generates weak acid surface groups which release CO at temperatures higher than 500 ºC.[54]

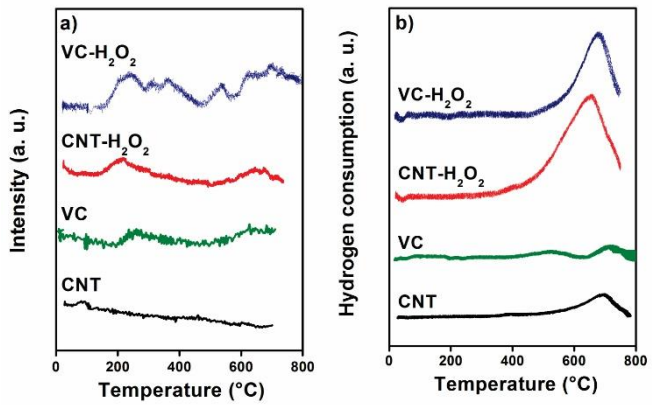

Figure 1. TPD (a) and TPR (b) profiles of carbon supports.

Table 1 shows the results of the textural and acid-basic characteristics of H_2O_2-functionalized and non-functionalized carbons. As it is observed, the surface area value for CNT and VC supports decreases after functionalization treatment in approximately 24 and 32%, respectively.

Table 1. Surface area (S_{BET}) and isoelectric points (IEP) of the carbons.

Support	S_{BET} (m^2 g^{-1})	IEP
CNT	211	7.0
VC	240	7.4
CNT-H_2O_2	160	6.6
VC-H_2O_2	162	6.3

Some authors[50,62-64] have reported the existence of diffusion restrictions in carbon micropores after other different chemical treatments. Therefore, the reduction of the surface area after H_2O_2 functionalization could be caused by the blockage of part of the micropores.

The isoelectric point (IEP) indicates the pH at which the surface possesses as many positive charges as negative ones. IEP results for the non-functionalized supports show an almost neutral pH value (7.0 and 7.4 for CNT and VC, respectively), which are in agreement with the TPD results that show practically no signals of desorption of acid functional groups (Fig. 1a). After functionalization with hydrogen peroxide, the IEP values decreased for both supports (6.6 and 6.3 for CNT and VC, respectively), a decline which is compatible with the development of acid functional groups detected by TPD (see also Fig. 1a). As previously shown[65], oxidation treatments generate a large amount of oxygenated groups (such as hydroxyl, carboxylic, and lactones) on the surface of the support. Such groups are able to modify both the pore structure and the acid-base character of the carbon.

Figure 1b shows temperature-programmed reduction (TPR) profiles of both functionalized and non-functionalized carbonaceous supports. The profiles of the non-functionalized supports do not practically present zones of hydrogen consumption, in agreement with the TPD results (Fig. 1a). In contrast, the profiles of the functionalized supports show H_2 consumption peaks at high temperatures, as a result of the reduction of weak oxygenated functional groups (C[O]). The appearance of this reduction zone was previously explained by de Miguel et al.[66]

The inductively coupled plasma–atomic emission spectrometry (ICP–AES) results indicates that PtSn/CNT, PtSn/CNT-H_2O_2, PtSn/VC, and PtSn/VC-H_2O_2 catalysts present Pt:Sn atomic ratios equal to 3.03, 3.01, 3.03, and 3.02, respectively.

Figures 2a and 2b show the temperature-programmed reduction profiles of the Pt and PtSn catalysts supported on CNT-H_2O_2 and VC-H_2O_2, respectively. For the sake of comparison, the profiles of the Pt/CNT-H_2O_2 and Pt/VC-H_2O_2 catalysts prepared by conventional impregnation (CI) method[50] are also shown.

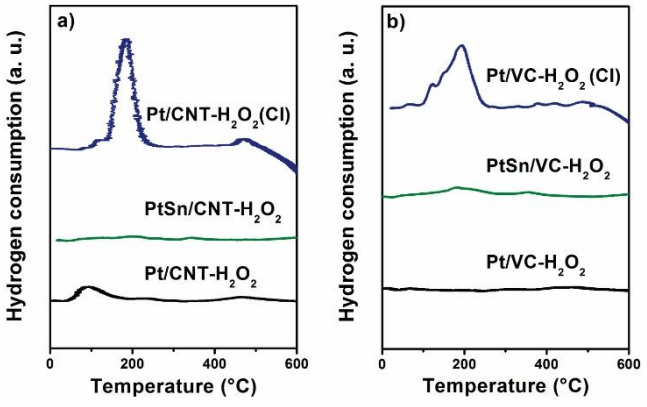

Figure 2. TPR profiles of Pt and PtSn catalysts supported on H_2O_2-functionalized CNT (a) and H_2O_2-functionalized VC (b).

It is observed that the TPR profiles of mono- and bimetallic catalysts prepared by the polyol method show practically no reduction peaks between 150 and 300 ºC, which is the zone where the Pt is reduced in the catalysts prepared by CI method. This fact could indicate that Pt is mostly found in its metallic state in the catalysts prepared by this method after the deposition-reduction step in liquid phase with EG. Regarding the

degree of Sn reduction, the absence of H_2 consumption peaks would be indicative that part of the promoter could have been co-reduced with Pt during the catalyst preparation.

The broad signals located at ca. 25º in the X-ray diffraction (XRD) patterns (Figure 3) correspond to CNT and VC materials, while the peaks located at 2Θ = 39º, 46º, and 68º correspond to (111), (200), and (220) planes of Pt, respectively.

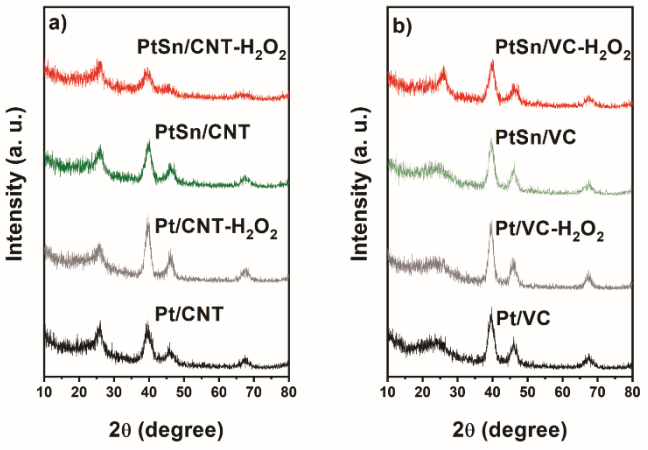

Figure 3. XRD profiles of Pt and PtSn catalysts supported on CNT and CNT-H_2O_2 (a) and VC and VC-H_2O_2 (b).

Table 2 presents the values of the medium crystallite sizes calculated according to Scherrer formula based on the (220) reflection of Pt. The values of the crystallite sizes are similar for all the catalysts, except for PtSn/CNT-H_2O_2, which is smaller than the other samples.

Table 2. Values of crystallite size determined by XRD from the widening of the (220) reflection of Pt, hydrogen chemisorption, and initial activity (R°_{Bz}) and activation energy (E_{aBz}) in benzene hydrogenation reaction for Pt and PtSn catalysts.

Catalyst	Crystallite size (nm)	H_2 chemisorption (μmol H_2 g cat^{-1})	R°_{Bz} (mol h^{-1} g Pt^{-1})	E_{aBz} (kcal mol^{-1})
Pt/CNT	3.6	308	2.33	7.9
Pt/CNT-H_2O_2	3.7	75	3.91	9.8
PtSn/CNT	3.4	318	0.75	11.4
PtSn/CNT-H_2O_2	2.4	470	1.70	23.9
Pt/VC	3.2	268	5.12	11.4
Pt/VC-H_2O_2	4.5	199	2.90	11.7
PtSn/VC	3.3	341	1.87	15.6
PtSn/VC-H_2O_2	3.5	395	1.24	16.7

In order to find more information about the Pt and Sn reducibilities of the bimetallic catalyst supported on CNT-H_2O_2, a XPS characterization was done as Figure 4 shows. From the deconvolution of Pt 4f spectra (Figure 4a) in the bimetallic catalyst, a peak at 71.9 eV was obtained for the Pt $4f_{7/2}$ signal and another peak at 75.2 eV for Pt $4f_{5/2}$. These peaks correspond to the zerovalent state of Pt. Two additional small doublets are also observed in Figure 4a, one at 74.3 eV and 77.8 eV and the other one at 75.5 eV and 79 eV, these corresponding to oxides or oxychlorides of Pt. Concerning the reduction degree of Pt in this bimetallic catalyst, most of the Pt was in a zerovalent state (60-70%) and a small portion was forming oxidized species of Pt (40-30%). From the deconvolution of the Sn 3d region of XPS spectra (Figure 4b), a small peak located at 485.4 eV is assigned to zerovalent Sn, and an important peak at 487.4 eV which is the characteristic peaks of Sn II/IV oxidized species. A very low amount of Sn(0) (12%) was found, with this small metallic fraction possibly forming alloys with metallic Pt. Similar results were found by Rodriguez et al.[39] This result indicates that Sn mainly exists in the form of SnO, SnO_2, or Sn hydroxides.

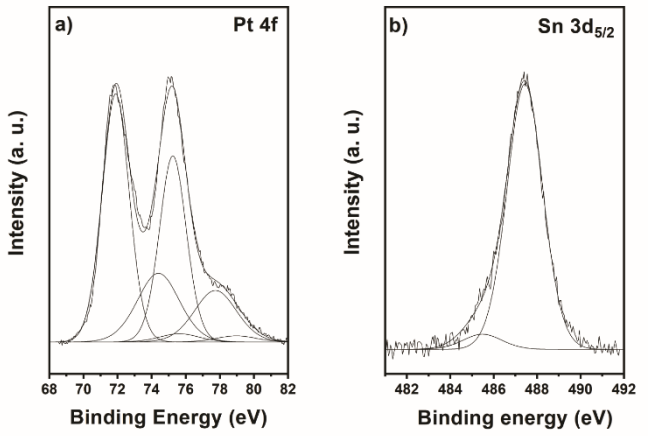

Figure 4. Pt 4f (a) and Sn $3d_{5/2}$ (b) XPS signals of PtSn/CNT-H_2O_2 catalyst.

Table 2 also shows hydrogen chemisorption capacities of both Pt and PtSn catalysts. PtSn catalysts supported on CNT-H_2O_2 and VC-H_2O_2 showed higher hydrogen chemisorption values than those of the corresponding monometallic ones (470 vs. 75 and 395 vs. 199 μmol H_2 g cat^{-1}, respectively). Such tendency is also observed for the PtSn/VC catalyst (341 vs. 268 μmol H_2 g cat^{-1}). These results are consistent with a decrease in particle size. On the contrary, for the bimetallic catalyst supported on CNT, hydrogen chemisorption value remains almost constant.

In order to characterize the metallic phase of catalysts, benzene hydrogenation, a structure-insensitive reaction, was used. In this test reaction, a probable modification of the activation energy could be due to an electronic change in the nature of the metallic site.[67] Table 2 shows the comparative values of initial activity (R°_{Bz}) measured at 110 ºC and activation energy (E_{aBz}) for the mono and bimetallic catalysts. It can be noted that the catalysts prepared on VC-H_2O_2 show lower values of initial activities, when compared to the corresponding ones prepared on VC. This fact could suggest that there is an important change in the interaction between the active metals and the support for Pt/VC-H_2O_2 and PtSn/VC-H_2O_2 catalysts, probably due to the influence of the groups generated during the functionalization with H_2O_2, which modify the adsorption mechanism of the metallic precursors on the support. However, this effect was not observed for the catalysts with the H_2O_2 functionalization on CNT support. For both catalyst series, a decrease in the activities of the bimetallic catalysts with respect to the corresponding monometallic ones is observed in Table 2, which

could be due to both geometric and electronic effects of the promoter (Sn) on the active metal (Pt).

An increase in E_{aBz} values is observed for the CNT-H_2O_2 and VC-H_2O_2 supported catalysts (mainly for the CNT-H_2O_2) compared to the non-functionalized ones. These changes suggest a modification in the active site-support interaction induced by the functionalization. In addition, the activation energy values of the PtSn catalysts are higher than those of the corresponding Pt catalysts. This fact would indicate the existence of electronic effects of Sn on the Pt active sites with probable alloy formation. Based on these results and taking into account that it is a test reaction of the metal phase insensitive to the structure, the existence of electronic effects could be inferred in these bimetallic catalysts prepared on carbon functionalized with hydrogen peroxide.

Transmission electron microscopy (TEM) was used to determine the particle size of the synthesized electrocatalysts. For each of them, a micrograph and the particle size distribution are shown (Figs. 5 and 6). The mean values of the particle size in each distribution are also presented. Bimetallic catalysts prepared on functionalized carbons show a homogeneous and narrow distribution of particle sizes. The mean diameters of the particles of PtSn/CNT-H_2O_2 and PtSn/VC-H_2O_2 catalysts are 2.3 and 3.4 nm, respectively. These results are in accordance with the crystallite sizes calculated by XRD and with the increase in the quantities of chemisorbed hydrogen found for the functionalized PtSn catalysts with respect to the corresponding monometallic ones (Table 2). It can be noted that both bimetallic catalysts prepared on functionalized carbons exhibit a decrease of the metallic particle in comparison to the corresponding monometallic catalyst. This fact would be in concordance with the results of the reaction tests of these catalysts, which exhibited a change in the promoter-active site-support interaction caused by the H_2O_2 functionalization treatment (Table 2).

CO stripping, as a structure-sensitive reaction[68-70] was adopted to evaluate the resistance to CO and electrochemical surface area (ECSA) of different catalysts. The ECSA values were calculated from the cyclic CO stripping voltammograms (see Figure S1) and are shown in Table 3. For monometallic catalysts prepared on functionalized supports, the CO oxidation initiation potentials appear at 0.27 and 0.28 V vs. Ag/AgCl (for CNT-H_2O_2 and VC-H_2O_2, respectively), while those for bimetallic catalysts are displaced towards lower values (0.14 V vs. Ag/AgCl, for both functionalized carbons). A clear promoter effect of Sn is observed in both cases, which shifts the CO oxidation peak to lower potentials. The presence of electronic effects of Sn on Pt, observed mainly in the test reaction of the metallic phase, would be responsible for this promoter effect. Note that CO oxidation occurs at a somewhat more negative potential for catalysts based on functionalized CNT and VC supports. These differences could be ascribed to changes in the surface characteristics of the catalysts.

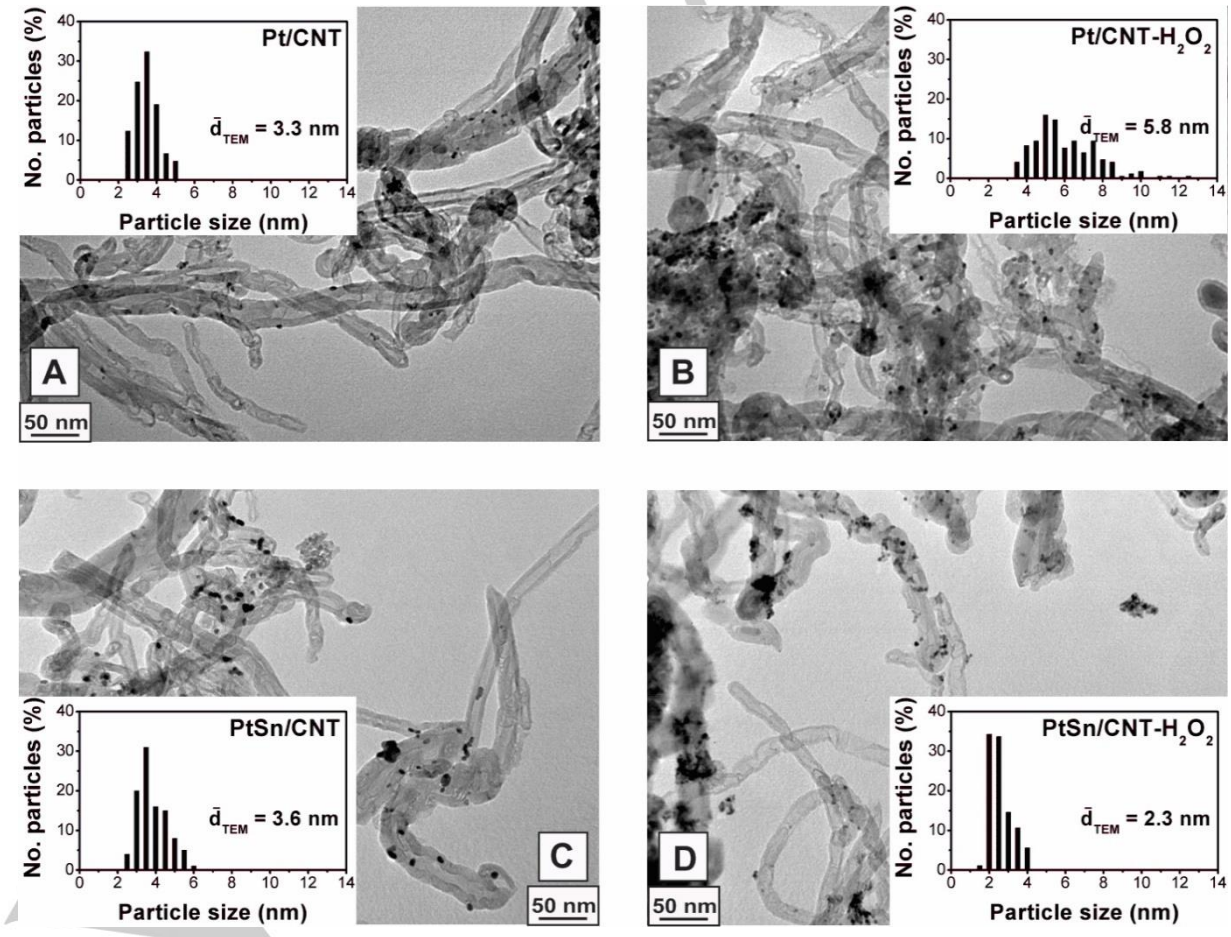

Figure 5. TEM images (A-D) of Pt and PtSn catalysts prepared on CNT and CNT-H_2O_2 with the corresponding particle size distribution histograms.

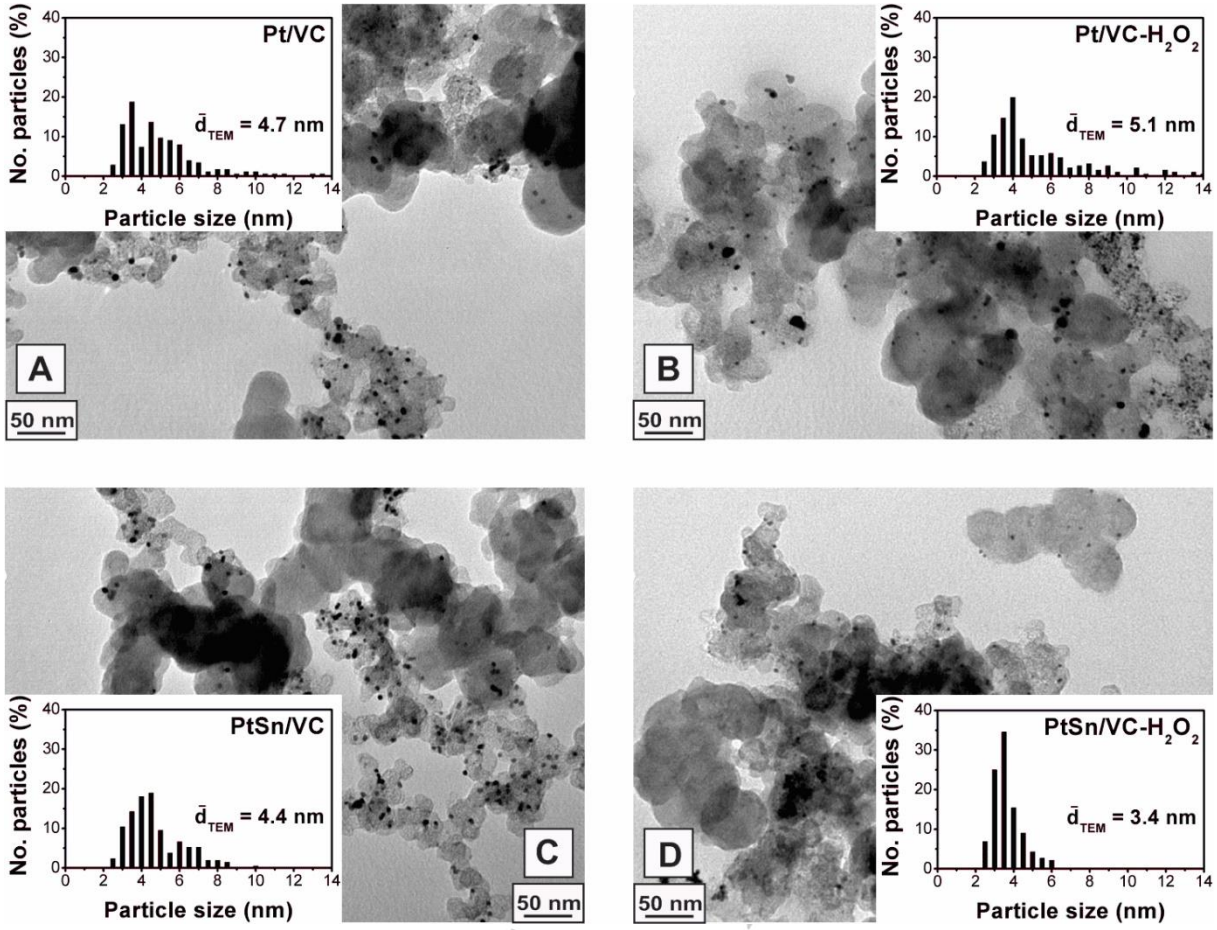

Figure 6. TEM images (A-D) of Pt and PtSn catalysts prepared on VCT and VC-H_2O_2 with the corresponding particle size distribution histograms.

Table 3. Onset potential of CO oxidation ($E_{CO,Onset}$) and electrochemical surface area (ECSA) from CO oxidation, and electrochemical performance of Pt and PtSn catalysts in EOR (peak potential and forward peak current from cyclic voltammetry).

Support	$E_{CO,Onset}$ (V vs Ag/AgCl)	ECSA (m^2 g Pt^{-1})	Peak potential (V vs Ag/AgCl)	Forward peak current (mA mg Pt^{-1})
Pt/CNT	0.43	12.2	0.73	50
Pt/CNT-H_2O_2	0.27	18.9	0.75	89
PtSn/CNT	0.17	30.0	0.77	175
PtSn/CNT-H_2O_2	0.14	67.8	0.82	380
Pt/VC	0.38	16.9	0.74	59
Pt/VC-H_2O_2	0.28	17.4	0.78	141
PtSn/VC	0.16	37.0	0.89	234
PtSn/VC-H_2O_2	0.14	44.4	0.88	296

The electrochemical surface area was estimated by calculating the areas of the peaks and the desorption amount of CO.[71] With the charge quantity $Q_{CO\text{-}adsorption}$, the ECSA value is calculated according to Eq. 1:

$$ECSA = \frac{Q_{CO-adsorption}(mC)}{0.42\ (mC\ gPt^{-1}) \times Pt\ loading\ (g\ cm^{-2})} \quad \text{(Eq. 1)}$$

where 0.42 (mC gPt^{-1}) represents the CO value of the amount of charge at the time the monolayer was adsorbed onto the Pt surface.[72]

Typically, the ECSA of PtSn/CNT-H_2O_2 catalyst was 67.8 m^2 g Pt^{-1}, which was 3.59, 2.26, and 5.56 times higher than the Pt/CNT-H_2O_2 (18.9 m^2 g Pt^{-1}), PtSn/CNT (30.0 m^2 g Pt^{-1}) and Pt/CNT (12.2 m^2 g Pt^{-1}) catalysts, in sequence. Considering VC support, the ECSA values of PtSn/VC-H_2O_2 catalyst was 44.4 m^2 g Pt^{-1}, being 2.55, 1.20, and 2.63 times higher than the Pt/VC-H_2O_2 (17.4 m^2 g Pt^{-1}), PtSn/VC (37.0 m^2 g Pt^{-1}) and Pt/VC (16.9 m^2 g Pt^{-1}) catalysts, respectively. From the results shown in Table 3, it can be inferred that the bimetallic catalysts supported on functionalized carbons have higher values of electrochemical areas than those of the corresponding monometallic ones, which agrees with the smallest nanoparticle size obtained in each series.

The catalytic activity of the catalysts was studied employing the cyclic voltammetry technique for the electrooxidation reaction of ethanol (Figure 7). The typical double irreversible wave is observed, associated with primary oxidation of ethanol and oxidative desorption of C_{Oads} and intermediate species generated at 0.82 and 0.88 V (vs. Ag/AgCl) for PtSn/CNT-H_2O_2 and PtSn/VC-H_2O_2, respectively, in the first wave.[73]

The presence of oxidized Sn species that form an oxide layer can produce a substantial modification of the electronic properties of the active sites. For PtSn/CNT-H_2O_2, PtSn/CNT, Pt/CNT-H_2O_2, PtSn/VC-H_2O_2, PtSn/VC, and Pt/VC-H_2O_2, a shoulder and an oxidation peak are observed in the backward scan, suggesting that the oxidation of two dissimilar species occurs in these electrocatalysts along with the ethanol direct oxidation. Nevertheless, these two oxidation peaks could also be related to ethanol oxidation at two different catalytic sites.[19]

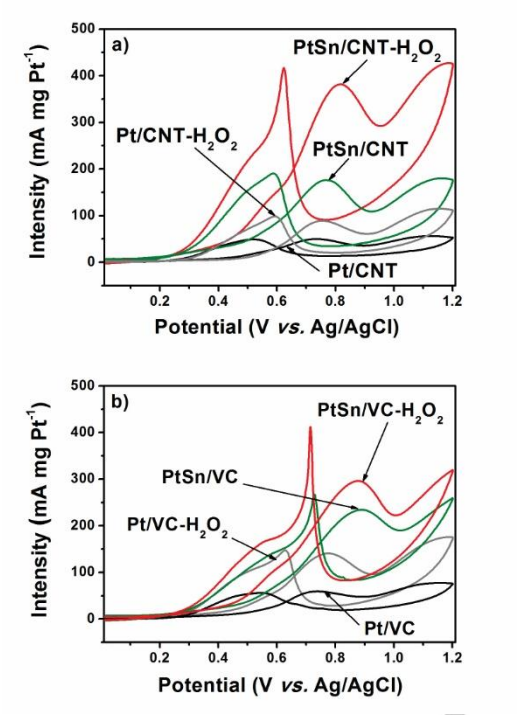

Figure 7. Cyclic voltammograms for EOR on Pt and PtSn catalysts prepared on CNT and CNT-H_2O_2 (a) and VC and VC-H_2O_2 (b), recorded in 0.5M H_2SO_4 + 1M C_2H_5OH electrolyte.

The highest current intensities are observed for PtSn catalysts supported on functionalized carbons, suggesting that the surface groups generated during the hydrogen peroxide treatment and the presence of a promoter like Sn can significantly improve the reaction rate. The PtSn/CNT-H_2O_2 catalyst current intensity is the highest of all prepared catalysts (380 mA mg Pt^{-1}), followed by the other bimetallic catalyst supported on functionalized Vulcan carbon (296 mA mg Pt^{-1}). The anodic peak current for both functionalized bimetallic catalysts occurs at 0.82 V and 0.88 V (vs. Ag/AgCl), respectively.

Chronoamperometric measurements were conducted to analyze the electrocatalytic activity and long-term stability. An initial period can be observed where the current decreases rapidly before 5 min followed by a slower decay, reaching a quasi-stationary within 60 min. Not only do bimetallic catalysts on H_2O_2-functionalized carbons have the highest current intensities but also good stability over time.

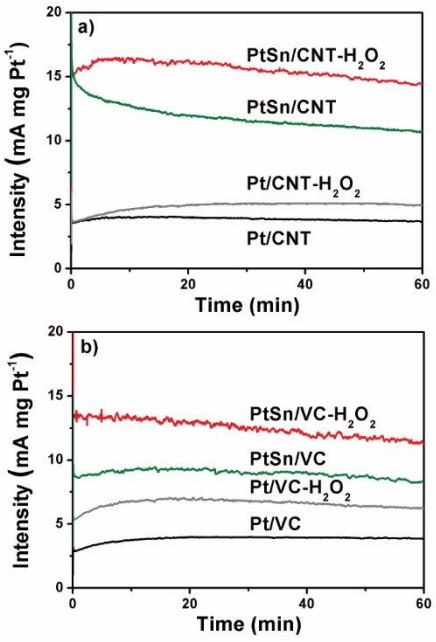

Figure 8. Chronoamperometry curves for EOR on Pt and PtSn catalysts prepared on CNT and CNT-H_2O_2 (a) and VC and VC-H_2O_2 (b), recorded in 0.5M H_2SO_4 + 1M C_2H_5OH electrolyte.

Conclusion

The polyol method was employed to prepare PtSn nanoparticles supported on multiwalled carbon nanotubes and Vulcan carbon. In addition to studying the influence of the promoter (Sn) on the active metal, the effect of functionalization of the supports with hydrogen peroxide was analyzed.

Specific surface areas of CNT and VC supports were reduced by 24% and 32%, respectively, after functionalization. H_2O_2 treatment led to substantial changes in the carbon structures. XRD results indicated that there was a change in the location of the peaks after functionalization. This effect can possibly be referred to the formation of oxygenated groups in the carbon structure. The modification of the surface of the carbon supports with H_2O_2 can increase the number of functional groups on the surface, thereby increasing the metallic dispersion of the bimetallic catalysts and hence decreasing metal particle size. In this sense, TEM images show a very homogeneous and uniform particle distribution for the PtSn/CNT-H_2O_2 and PtSn/VC-H_2O_2 catalysts.

The results of cyclic voltammetry reveal that the presence of functional groups in the supports and the addition of a good promoter such as Sn to Pt improve the electrocatalytic activity towards the oxidation of ethanol.

The bimetallic catalysts supported on H_2O_2-functionalized CNT and VC showed higher electrochemical surface areas than those of the corresponding catalysts prepared on non-functionalized supports. The changes in the metal-support interaction due to the presence of functional groups in the carbons and the Pt-promoter interaction could lead to a better electrochemical behavior, not only in activity but also in stability.

Carbon functionalized with H_2O_2 developed acid sites and presented a strong interaction with the metal precursors during the preparation. This fact enhances (in the bimetallic catalysts) the metallic dispersion and consequently the electrocatalytic

behavior. The best performance for the ethanol electrooxidation was obtained with the PtSn/CNT-H_2O_2 catalyst, achieving a current intensity of 380 mA mg Pt^{-1}.

Experimental Section

Materials

Multiwalled carbon nanotubes (CNT) from Sunnano and Vulcan XC-72 (VC) from Cabot were used as supports. The precursors employed to prepare the anode catalysts were $H_2PtCl_6.6H_2O$ (Merck) and $SnCl_2.2H_2O$ (Cicarelli). Ethylene glycol (EG) from Merck was used as reducing agent. Nafion® (DuPont) and acetone (Merck) were employed to make catalyst ink. Ethanol and H_2SO_4 (both from Merck) were used as fuel and electrolyte for electrochemical measurements.

Support Purification

Prior to synthesis, CNT were purified to remove all inorganic impurities according to the procedure presented by Vilella et al.[74] Vulcan carbon was not purified because the amount of impurities present in the support was negligible.

Support Functionalization

Both CNT and VC supports were functionalized. Carbons were added into an H_2O_2 solution (30 %v/v) at room temperature and maintained for 48 h under stirring. Samples were filtered, washed with plenty of water and dried overnight at 110 °C in order to obtain the H_2O_2-functionalized carbons, which were named as CNT-H_2O_2 and VC-H_2O_2.

Catalyst Preparation

Supported Pt and PtSn catalysts were prepared by polyol method.[75] Carbon supports were dispersed into a 75:25 (v/v) mixture of EG and water and ultrasonicated for 30 min to afford a homogeneous suspension. Then, Pt and Sn precursors were added under stirring. Such suspension was transferred into a flask with a condenser and maintained under reflux for 2 h. Finally, the catalysts were filtered, thoroughly washed with plenty of water, and dried overnight at 70 ºC. For each of the samples, Pt and Sn contents were 20 wt.% and 4.06 wt.%, respectively. For the sake of comparison, Pt and PtSn catalysts over non-functionalized carbons were also prepared.

Structural Characterization

The specific surface area values of the carbons were measured by N_2 gas adsorption at -196 ºC with an automated adsorption sortometer (Quantachrome Corporation NOVA-1000). Isoelectric points of carbons were determined by neutralization at constant pH in a KNO_3 solution under N_2 atmosphere. Temperature-programmed desorption and temperature-programmed reduction experiments were carried out in an apparatus described elsewhere.[33] For TPD measurements, carbon supports were heated from 25 to 750 ºC (6 ºC min^{-1}) under He flow (9 mL min^{-1}). For TPR measurements, samples were reduced by a reductive mixture (10 mL min^{-1} of H_2 (5 vol%)-N_2) from 25 to 800 ºC (6 ºC min^{-1}). The catalyst morphology, distribution, and particle sizes were obtained using JEOL 100CX-TEM (high-resolution transmission electron microscopy). X-Ray Diffraction profiles were collected using a Shimadzu XD3A diffractometer with CuKα radiation (1.542 Å, 30kV and 40 mA). The X-ray photoelectron spectroscopy (XPS) analysis was performed on a Multitecnica Specs equipment, with a dual Ag/Al monochromatic X-ray source and a PHOIBOS 150 hemispherical analyzer. Spectra were obtained with AlKα monochromatic radiation at 300 W. The step energy was 30 eV and the fixed analyzer transmission mode (FAT) was used. The chemisorption of hydrogen was performed in a static glass volumetric apparatus at room temperature. The sample was previously outgassed at 100 ºC for 30 min. Details of the method are described in Veizaga et al.[40] Catalytic activity for benzene (Bz) hydrogenation reaction was determined in a differential flow reactor at 90, 100, and 110 ºC, using an H_2/Bz molar ratio equal to 26 with a volumetric flow of 600 mL min^{-1}. Benzene and cyclohexane were analyzed by gas chromatography. Actual content of Pt and Sn in the electrocatalysts was obtained using inductively coupled plasma–atomic emission spectrometry (ICP–AES) technique with an OPTIMA 3000 (Perkin Elmer Co.).

Electrochemical Measurements

For electrochemical characterization, a three-electrode test cell (Pine) was employed. The working electrode consists of a thin layer of Nafion impregnated catalyst composite cast on a vitreous carbon disk electrode. A Pt foil was used as counter electrode and an Ag/AgCl electrode as reference electrode. Oxygen was removed in the electrolyte solution before measurements by means of an ultra-pure N_2 flow during 15 min. To achieve a thin and uniform dispersion of catalysts on the vitreous carbon substrate of 4 mm diameter, the following procedure was employed. Each catalyst powder (20 mg) was dispersed in a Nafion/acetone dispersion (7 %v/v) and ultrasonicated for 15 min. The resulting dispersion (8 µL) was cast on the working electrode substrate and dried for 5 min. Cyclic voltammetry measurements were conducted in 0.5M H_2SO_4 + 1M C_2H_5OH solution with a scan rate of 0.025 V s^{-1}. Chronoamperometric tests were carried out in 0.5M H_2SO_4 + 1M C_2H_5OH solution at 0.35 V vs. Ag/AgCl for 60 min. In CO stripping measurements, CO was adsorbed on each electrode by immersing them in a 0.5M H_2SO_4 solution saturated with CO for 1 h at a constant potential of 0.2 V vs. Ag/AgCl. The excess CO was eliminated by N_2 bubbling. Stripping charge was evaluated from a voltammogram between -0.2 and 1.2 V vs. Ag/AgCl at a sweep rate of 0.025 V s^{-1}.

Acknowledgements

Authors acknowledge Universidad Nacional del Litoral (Project CAI+D) and CONICET (Project PUE) for their financial support.

Keywords: carbon supports • direct ethanol fuel cells • hydrogen peroxide functionalization • polyol method • PtSn electrocatalysts

[1] S.P.S. Badwal, S. Giddey, A. Kulkarni, J. Goel, S. Basu, *Appl. Energy* **2015**, *145*, 80-103.
[2] B.C. Ong, S.K. Kamarudin, S. Basri, *Int. J. Hydrog. Energy* **2017**, *42*, 10142-10157.
[3] N. Sazali, W.N. Wan Salleh, A.S. Jamaludin, M.N. Mhd Razali, *Membranes* **2020**, *10*, 99.
[4] Y. Wang, D.F. Ruiz Diaz, K.S. Chen, Z. Wang, X.C. Adroher, *Mater. Today* **2020**, *32*, 178-203.
[5] Y. Zheng, X. Wan, X. Cheng, K. Cheng, Z. Dai, Z. Liu, *Catalysts* **2020**, *10*, 166.
[6] L. Yaqoob, T. Noor, N. Iqbal, *RSC Advances* **2021**, *11*, 16768-16804.
[7] Y. Zhang, F. Gao, H. You, Z. Li, B. Zou, Y. Du, *Coord. Chem. Rev.* **2022**, *450*, 214244.
[8] S.S. Siwal, S. Thakur, Q.B. Zhang, V.K. Thakur, *Mater. Today Chem.* **2019**, *14*, 100182.
[9] M.C. Figueiredo, O. Sorsa, N. Doan, E. Pohjalainen, H. Hildebrand, P. Schmuki, B.P. Wilson, T. Kallio, *J. Power Sources* **2015**, *275*, 341-350.
[10] M.A.F. Akhairi, S.K. Kamarudin, *Int. J. Hydrog. Energy* **2016**, *41*, 4214-4228.
[11] Y.V. Tolmachev, O.A. Petrii, *J. Solid State Electrochem*. **2017**, *21*, 613-639.

[12] J.E. Sulaiman, S. Zhu, Z. Xing, Q. Chang, M. Shao, *ACS Catal*. **2017**, *7*, 5134-5141.
[13] S.S. Gwebu, P.N. Nomngongo, N.W. Maxakato, *Electroanalysis* **2018**, *30*, 1125-1132.
[14] Y. Liu, M. Wei, D. Raciti, Y. Wang, P. Hu, J. H. Park, M. Barclay, C. Wang, *ACS Catal.* **2018**, *8*, 10931-10937.
[15] S.-Y. Yan, Y.-R. Huang, C.-Y. Yang, C.-W. Liu, J.-H. Wang, K.-W. Wang, *Electrochim. Acta* **2018**, *259*, 733-741.
[16] F. Colmati, M.M. Magalhães, R. Sousa Jr., E.G. Ciapina, E.R. Gonzalez, *Int. J. Hydrog. Energy* **2019**, *44*, 28812-28820.
[17] Z. Gu, S. Li, Z. Xiong, H. Xu, F. Gao, Y. Du, *J. Colloid Interface Sci.* **2018**, *521*, 111-118.
[18] N. Mahamai, T. Prom-anan, T. Sarakonsri, *Mater. Today: Proc.* **2019**, *17*, 1561-1568.
[19] N.S. Veizaga, G. Mendow, A.F. Quintero-Jaime, E. Morallón, D. Cazorla-Amorós, *Mater. Chem. Phys*. **2022**, *275*, 125282.
[20] E. Antolini, *Appl. Catal. B: Environ*. **2007**, *74*, 324-336.
[21] X. Wang, F. Zhu, Y. He, M. Wang, Z. Zhang, Z. Ma, R. Li, *J. Colloid Interface Sci.* **2016**, *468*, 200-210.
[22] N. Hidayati, K. Scott, *Bull. Chem. React. Eng. Catal*. **2016**, *11*, 10-20.
[23] E. Antolini, *Energies* **2017**, *10*, 42.
[24] S.-H. Han, H.-M. Liu, P. Chen, J.-X. Jiang, Y. Chen, *Adv. Energy Mater*. **2018**, *8*, 1801326.
[25] F. Ginez Carbajal, M.A. García, S.A. Gamboa, *J. New Mat. Electrochem. Sys.* **2018**, *21*, 43-49.
[26] P.G. Corradini, N.A. Santos, J. Perez, *Fuel Cells* **2018**, *18*, 73-81.
[27] S. Dai, T.-H. Huang, X. Yan, C.-Y. Yang, T.-Y. Chen, J.-H. Wang, X. Pan, K.-W. Wang, *ACS Energy Lett*. **2018**, *3*, 2550-2557.
[28] T.-H. Huang, H.-S. Zheng, Y.-M. Cheng, C.-W. Liu, S.-W. Lee, J.-H. Wang, K.-W. Wang, *Sustain. Energy Fuels* **2019**, *3*, 3352-3362.
[29] N. Mahamai, T. Sarakonsri, *Solid State Phenom*. **2020**, *302*, 37-43.
[30] C. Wang, H. Xu, F. Gao, Y. Zhang, T. Song, C. Wang, H. Shang, X. Zhu, Y. Du, *Nanoscale* **2019**, *11*, 18176-18182.
[31] C. Chen, H. Xu, H. Shang, L. Jin, T. Song, C. Wang, F. Gao, Y. Zhang, Y. Du, *Nanoscale* **2019**, *11*, 20090-20095.
[32] F. Gao, Y. Zhang, B. Zou, F. Jiang, Z. Li, Y. Du, *J. Colloid Interface Sci.* **2022**, *610*, 271–279.
[33] W. Zhou, Z. Zhou, S. Song, W. Li, G. Sun, P. Tsiakaras, Q. Xin, *Appl. Catal. B Environ*. **2003**, *46*, 273-285.
[34] C. Lamy, S. Rousseau, E.M. Belgsir, C. Coutanceau, J.-M. Léger, *Electrochim. Acta* **2004**, *49*, 3901-3908.
[35] S.C. Zignani, V. Baglio, J.J. Linares, G. Monforte, E.R. Gonzalez, A.S. Aricò, *Electrochim. Acta* **2012**, *70*, 255-265.
[36] S.G. Ramos, A. Calafiore, A.R. Bonesi, W.E. Triaca, A.M. Castro Luna, M.S. Moreno, G. Zampieri, S. Bengio, *Int. J. Hydrogen Energy* **2012**, *37*, 14849-14853.
[37] S. Beyhan, C. Coutanceau, J.-M. Léger, T. Napporn, F. Kadırgan, *Int. J. Hydrogen Energy* **2013**, *38*, 6830-6841.
[38] N.S. Veizaga, V.I. Rodriguez, T.A. Rocha, M. Bruno, O.A. Scelza, S.R. de Miguel, E.R. Gonzalez, *J. Electrochem. Soc.* **2015**, *162*, F243-F249.
[39] V.I. Rodriguez, N.S. Veizaga, S.R. de Miguel, *J. Electrochem. Soc.* **2017**, *164*, F1524-F1533.
[40] R. Rizo, D. Sebastián, M.J. Lázaro, E. Pastor, *Appl. Catal. B: Environ.* **2017**, *200*, 246-254.
[41] A. Sandoval-González, S.A. Gamboa, *J. New Mater. Electrochem. Syst.* **2018**, *21*, 21-28.
[42] Z.A.C. Ramli, S.K. Kamarudin, *Nanoscale Res. Lett.* **2018**, *13*, 410.
[43] M.F. Azcoaga Chort, P.A. Nagel, N.S. Veizaga, V.I. Rodríguez, S.R. de Miguel, *Can. J. Chem. Eng.* **2022**, *100*, 1848-1857.
[44] B. Hasa, E. Martino, S. Tsatsos, J. Vakros, G. Kyriakou, A. Katsaounis, *J. Appl. Electrochem.* **2022**, *52*, 509-520.
[45] M. Carmo, M. Linardi, J.-G. Rocha Poco, *Int. J. Hydrog. Energy* **2008**, *33*, 6289-6297.
[46] J.R.C. Salgado, J.C.S. Fernandes, A.M. Botelho do Rego, A.M. Ferraria, R.G. Duarte, M.G.S. Ferreira, *Electrochim. Acta* **2011**, *56*, 8509-8518.
[47] C. Alegre, M.E. Gálvez, E. Baquedano, R. Moliner, E. Pastor, M.J. Lázaro, *J. Phys. Chem. C* **2013**, *117*, 13045-13058.
[48] Y.-C. Chiang, M.-K. Hsieh, H.-H. Hsu, *Thin Solid Films* **2014**, *570*, 221-229.
[49] M. Steimecke, S. Rümmler, M. Bron, *Electrochim. Acta* **2015**, *163*, 1-8.
[50] N.S. Veizaga, V.I. Rodriguez, S.R. de Miguel, *J. Electrochem. Soc.* **2017**, *164*, F22-F31.
[51] E.M.I. Elsehly, N.G. Chechenin, A.V. Makunin, H.A. Motaweh, E.G. Leksina, *Water Sci. Technol.* **2017**, *75*, 1564-1571.
[52] N. Sezer, M. Koç, *Surf. Interfaces* **2019**, *14*, 1-8.
[53] Y.-W. Chen, H.-G. Chen, M.-Y. Lo, Y.-C. Chen, *Materials* **2021**, *14*, 3902.
[54] S.R. de Miguel, M.C. Román-Martinez, E. Jablonski, J.L.G. Fierro, D. Cazorla-Amorós, O.A. Scelza, *J. Catal.* **1999**, *184*, 514-525.
[55] Z. Tian, C. Liu, Q. Li, J. Hou, Y. Li, S. Ai, *Appl. Catal. A: Gen.* **2015**, *506*, 134-142.
[56] W. Yu, Z. Xin, W. Zhang, Y. Xie, J. Wang, S. Niu, Y. Wu, L. Shao, *Chem. Phys. Lett.* **2017**, *686*, 155-160.
[57] B. Zhong, H. Liu, X. Gu, D.S. Su, *ChemCatChem* **2014**, *6*, 1553-1557.
[58] S. Yang, X. Wang, H. Yang, Y. Sun, Y. Liu, *J. Hazard. Mater.* **2012**, *233*, 18-24.
[59] R. Marega, G. Accorsi, M. Meneghetti, A. Parisini, M. Pratoa, D. Bonifazi, *Carbon* **2009**, *47,* 675-682.
[60] F. Avilés, J.V. Cauich-Rodríguez, L. Moo-Tah, A. May-Pat, R. Vargas-Coronado, *Carbon* **2009**, *47*, 2970-2975.
[61] I.A. Safo, F. Liu, K. Xie, W. Xia, *Mater. Chem. Phys*. **2018**, *214*, 472-481.
[62] M. Carmo, M. Brandalise, A. Oliveira Neto, E.V. Spinacé, A.D. Taylor, M. Linardi, J.G. Rocha Poço, *Int. J. Hydrog. Energy* **2011**, *36*, 14659-14667.
[63] J.L. Reyes-Rodríguez, K. Sathish-Kumar, O. Solorza-Feria, *Int. J. Hydrog. Energy* **2015**, *40*, 17253-17263.
[64] S. Jongsomjit, K. Sombatmankhong, P. Prapainainar, *RSC Adv.* **2015**, *5*, 61298-61308.
[65] M. Carmo, M. Linardi, J.G. Rocha Poco, *Appl. Catal. A: Gen.* **2009**, *355*, 132-138.
[66] S.R. de Miguel, O.A. Scelza, M.C. Roman-Martinez, C. Salinas Martinez de Lecea, C., D. Cazorla-Amoros, A. Linares-Solano, *Appl. Catal. A: Gen.* **1998**, *170*, 93-103.
[67] D. Poondi, M.A. Vannice, *J. Catal.* **1996**, *161*, 742-751.
[68] S. Garcia-Rodriguez, F. Somodi, I. Borbáth, J.L. Margitfalvi, M.A. Peña, J.L.G. Fierro, S. Rojas, *Appl. Catal. B: Environ.* **2009**, *91*, 83-91.
[69] M. Arenz, V. Stamenkovic, B.B. Blizanac, K.J. Mayrhofer, N.M. Markovic, P.N. Ross, *J. Catal.* **2005**, *232*, 402-410.
[70] V. Stamenkovic, M. Arenz, B.B. Blizanac, K.J.J. Mayrhofer, N.M. Markovic, P.N. Ross, *Surf. Sci.* **2005**, *576*, 145-157.
[71] T. Vidaković, M. Christov, K. Sundmacher, *Electrochim. Acta* **2007**, *52*, 5606-5613.
[72] F. Maillard, S. Schreier, M. Hanzlik, E.R. Savinova, S. Weinkauf, U. Stimming, *Phys. Chem. Chem. Phys* **2005**, *7*, 385-393.
[73] Y. Xu, A. Amini, M. Schell, *J. Electroanal. Chem.* **1995**, *398*, 95-104.
[74] I.M.J. Vilella, S.R. de Miguel, C. Salinas-Martínez de Lecea, Á. Linares-Solano, O.A. Scelza, *Appl. Cat. A Gen.* **2005**, *281*, 247-258.
[75] E.V. Spinacé, R.R. Dias, M. Brandalise, M. Linardi, A. Oliveira Neto, *Ionics* **2010**, *16*, 91-95.

Entry for the Table of Contents

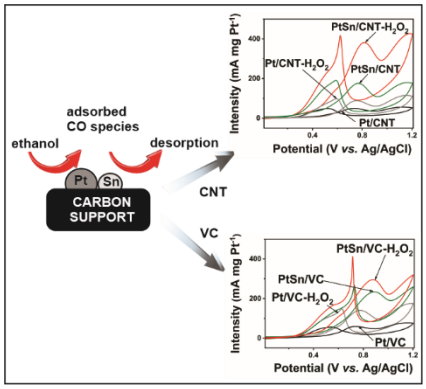

H_2O_2 treatment caused substantial modifications in the carbon structures. Changes in the metal-support interaction led to improved electrochemical behavior. A clear promoter effect of Sn is observed in both functionalized carbons, which shifts the CO oxidation peak to lower potentials. The current intensity of PtSn/CNT-H_2O_2 catalyst is the highest of all prepared catalysts (380 mA mg Pt^{-1}), followed by the other bimetallic catalyst supported on functionalized Vulcan carbon (296 mA mg Pt^{-1}).